LASER & PHOTONICS REVIEWS
www.lpr-journal.org

Speckle-Insensitive Fractal Superconducting Nanowire Single-Photon Detector Coupled with Multimode Optical Fiber

*Kai Zou, Yun Meng, Zifan Hao, Song Li, Adrian Iovan, Thomas Descamps, Val Zwiller, and Xiaolong Hu**

Speckles are ubiquitous phenomena associated with multi-spatial-mode optics, which may reduce detection efficiency and induce modal noise if the photoresponse of the detector is polarization-dependent. Thus far, they limit the performance of superconducting nanowire single-photon detectors (SNSPDs) coupled with multimode optical fibers (MMF). To solve this problem, here, it is shown that SNSPDs patterned into the fractal geometry is insensitive to speckles and generates minimal modal noise that would otherwise be induced by the polarization-dependent local device efficiency of the meander and spiral SNSPDs. Using this advantageous property of the fractal SNSPDs, 78 ± 2% system detection efficiency at the wavelength of 1530 nm and 42-ps timing jitter is demonstrated when we couple a fractal SNSPD with 50-micrometer-core, step-index MMF. This work not only demonstrates a scheme to achieving high system detection efficiency for MMF-coupled SNSPDs that can be used in many applications, but also provides insight on how engineered nanostructures of photodetectors can reduce modal noise when detecting light from multiple spatial modes.

1. Introduction

Superconducting nanowire single-photon detectors (SNSPDs), or, also referred to as superconducting strip photon detectors (SSPDs), have played vital roles in many classical and quantum photonic applications.[1–4] After research and development in the past more than twenty years,[5] system detection efficiency (SDE) of the SNSPDs coupled with single-mode optical fibers (SMFs) has exceeded 90% or has even approached near 100% in several spectral bands.[6–10] However, the numerical aperture (NA) of SMF is small, and therefore, the SMF-coupled SNSPDs are more suitable for applications where the to-be-detected photons have already been coupled into SMFs.[3] Otherwise, if the incident photons are from free space[11] or from multimode optical fibers (MMF),[12] the limited NA of SMF would result in low receiving efficiency, η_r. Therefore, in the applications such as fluorescence-lifetime microscopy,[13,14] remote sensing,[11,15] photon-counting optical communications,[16] characterization of quantum dots,[17] and quantum communications via MMFs,[18] MMF-coupled SNSPDs are preferable. In these scenarios, for photon-starved applications in particular, we need to achieve high η_r while simultaneously maintaining other merits of high SDE, low dark-count rate (DCR), fast operating speed, and high timing resolution to fully unlock the potentials of the SNSPDs.

Although several research groups have explored MMF-coupled SNSPDs,[19–23] the reported SDE has been ranging from 18% to 71%. Several challenges exist, and need to be addressed in order to achieve high SDE. 1) Large-area SNSPDs are needed to achieve high coupling efficiency with MMF, η_c, while the device efficiency, $\eta_D = A \times P_r$, itself should also be high, where A is overall optical absorptance and P_r is overall internal detection efficiency. This requirement poses challenges on nanofabrication of the constriction (defect)-free devices.[24] Additionally, expanding the photosensitive area may worsen the properties in the time domain including operating speed and timing jitter.[25–27] 2) More importantly, the speckles in the MMF limit η_D of the SNSPDs in most commonly used the nanowire-meander device structure. Speckles are ubiquitous phenomena in multi-spatial-mode coherent optical systems,[28,29] and they are the consequence of interference of the modes with phase differences. In MMFs, speckles make the spatial distributions of local intensity and states of polarization (SoP) random, and these distributions are sensitive to external perturbations to the MMFs. Because local device efficiency, η_d (both local optical absorptance, a, and local internal detection efficiency, p_r[30]), of the superconducting nanowire is

K. Zou, Y. Meng, Z. Hao, S. Li, X. Hu
School of Precision Instrument and Optoelectronic Engineering
Tianjin University
Tianjin 300072, China
E-mail: xiaolonghu@tju.edu.cn
K. Zou, Y. Meng, Z. Hao, S. Li, X. Hu
Key Laboratory of Optoelectronic Information Science and Technology
Ministry of Education
Tianjin 300072, China
A. Iovan, T. Descamps, V. Zwiller
Department of Applied Physics
Royal Institute of Technology (KTH)
Stockholm SE-106 91, Sweden
The ORCID identification number(s) for the author(s) of this article can be found under https://doi.org/10.1002/lpor.202400342

DOI: 10.1002/lpor.202400342

dependent on the SoP, η_D would be an average of distributed, high and low η_d responding to the speckles. Therefore, in order to achieve high SDE for a MMF-coupled SNSPD, ideally, we need to make η_d high across the entire photosensitive region regardless of the distribution of the speckle patterns. We term this requirement being speckle-insensitive, which is the key in principle to achieving high SDE for MMF-coupled SNSPDs.

Fractal SNSPDs were introduced in 2015,[31] and in the past, we demonstrated that fractal SNSPDs coupled with SMFs[32,33] and achieved combined merits of high SDE, low polarization sensitivity (PS), and low timing jitter.[10,34] In this work, we show that SNSPDs patterned into the fractal geometries are insensitive to speckles when they are coupled with MMFs. In comparison, we show that the meander SNSPDs[7–9] and spiral SNSPDs[35,36] are sensitive to speckles and cannot achieve high A, or high η_D, although the latter is considered to be a polarization-insensitive design for the SMF-coupled scenario.[36] Furthermore, we find that modal noise[29] of the fractal SNSPDs, due to the speckle-induced changes in A, is significantly lower, compared with the modal noise of the meander and spiral SNSPDs. To our knowledge, prior to our work, modal noise associated with SNSPDs has never been studied before. After illustrating these important properties of the fractal SNSPDs, and with careful design, optimization, and implementation, we demonstrate $78 \pm 2\%$ SDE at the wavelength of 1530 nm, when the fractal SNSPD is coupled with a 50-μ m-core, step-index MMF, and timing jitter was measured to be 42 ps. We note that the demonstrated SDE is the highest among SDE of MMF-coupled SNSPDs reported so far in this wavelength range. Our work not only demonstrates a very useful scheme to achieving efficient MMF-coupled SNSPDs for various applications, but also provides insight on how carefully engineered nanostructures of photodetectors can reduce the modal noise[29] when the photodetectors detect light in multiple spatial modes.

2. Concept and Principle

We illustrate how the speckles at the output facet of the MMF affect optical absorptance, A, of the SNSPDs patterned into different geometries. To this end, we set up a simplified, but effective model to reduce the demand of computer memories and simulation time for the MMF. The model consists of a cylindrical dielectric waveguide with a core diameter of 10 μ m, optical refractive indices of the core and cladding layers to be 1.45 and 1.00 at 1550 nm, respectively. See Section SI (Supporting Information). This waveguide supports 236 guiding modes in total. For the SNSPDs, we considered three geometries (**Figure 1a**): 1) an arced-fractal Peano curve, 2) a meander, and 3) a spiral. We kept the width, 100 nm, and the fill factor, 0.26, identical for the three geometries. We used the microcavities with distributed Bragg reflectors (DBRs)[34] for enhancing optical absorption. The design of the microcavity for each geometry optimizes A assuming the incident photons in HE_{11y} mode (V) of a standard SMF. Table S1 (Supporting Information) presents the parameters of the multimode waveguide and the SNSPDs used in the simulation. To simulate the speckles, we superposed the first 20 vectorial modes with random amplitudes, c^m and random phases, Φ^m. $\mathbf{E}(x,y) = \sum_{m=1}^{20} c^m \mathbf{E}^m(x,y) e^{j\Phi^m} = E_x\hat{\mathbf{x}} + E_y\hat{\mathbf{y}}$. We simulated the optical absorptance, A, of the fractal, meander, and spiral SNSPDs under 30 cases of superposition. Figure 1b presents an example (case 1) of the simulated distribution of Stokes parameters, $S_0 = |E_x|^2 + |E_y|^2$, $S_1 = \left(|E_x|^2 - |E_y|^2\right)/S_0$, $S_2 = 2\Re(E_x E_y^*)/S_0$, $S_3 = -2\Im(E_x E_y^*)/S_0$, of the light in the waveguide, where E_x and E_y are the x and y components of the electrical field, respectively, and Figure 1c presents these parameters of another example (case 2).

The simulation results of optical absorptance, A, show that the nanowire patterned into the fractal geometry is, in principle, insensitive to speckles, and can achieve high optical absorption with negligibly low fluctuations. Figure 1d presents the simulated optical absorptance of the SNSPDs in three geometries integrated the optimized cavities. For the 30 cases, the average A with the microcavity is $\bar{A} = 0.90$, and the standard deviation, σ_A, is 0.01, for the fractal SNSPD. In comparison, the nanowires patterned into the meander and spiral geometries does not exhibit the merit of high optical absorption and low standard deviation, even if the spiral SNSPD is polarization insensitive when it is coupled with the standard SMF.[36] Table S2 (Supporting Information) lists the simulated $\bar{A}$ and σ_A for the MMF-coupled cases, as well as A for the SMF-coupled cases. From the point of view of effective-medium theory, the fractal nanowire can be treated as a homogenized photosensitive region with no particular global orientations, the local optical absorptance, a, and therefore, its areal integral, A, is independent of the speckle patterns and the local polarization. In comparison, the meander and the spiral ones do have a global orientation in each case. The spatial overlap integral with the speckles with random SoP results in reduced, average optical absorptance, A, and generates prominent fluctuation, σ_A, when the speckle pattern changes. Consequently, more modal noise is generated. We note that this effect, geometry-dependent optical absorptance, is not due to the microcavity. We also present in Figure 1e the optical absorptance of the assumed, free-standing SNSPDs in three geometries, and observe the same effect. By taking into account even more spatial modes, for example, 50 modes and 100 modes, in the simulation, we also observe the same effect. See Section SI (Supporting Information) for more details. We also note that we only simulate A here, but the similar effect should occur on P_r, because P_r is also polarization-dependent.[30]

3. Experimental Results

We fabricated fractal SNSPDs with an expanded photosensitive area, 22.9 μ m × 22.9 μ m, which was approximately four times larger than those we made for SMF coupling[10,34] (see Experimental Section). The scanning electron micrograph is presented in **Figure 2a**. The device was configured into a 36 cascaded superconducting nanowire avalanche photodetector (SNAP), and the width of nanowire was 50 nm, as shown in Figure 2b. The equivalent electrical circuitry of this detector is presented in Figure S4 (Supporting Information). The slightly increased width from 40 nm that we typically used[10,34] helped reduce the constrictions and might increase the yield of the devices with larger areas. For coupling with the MMF, we used the dual-lens coupling scheme[20] with a beam compression ratio of 0.37. Figure 2c presents the schematic of the design. An optical filter may be used in the package to suppress the dark counts induced

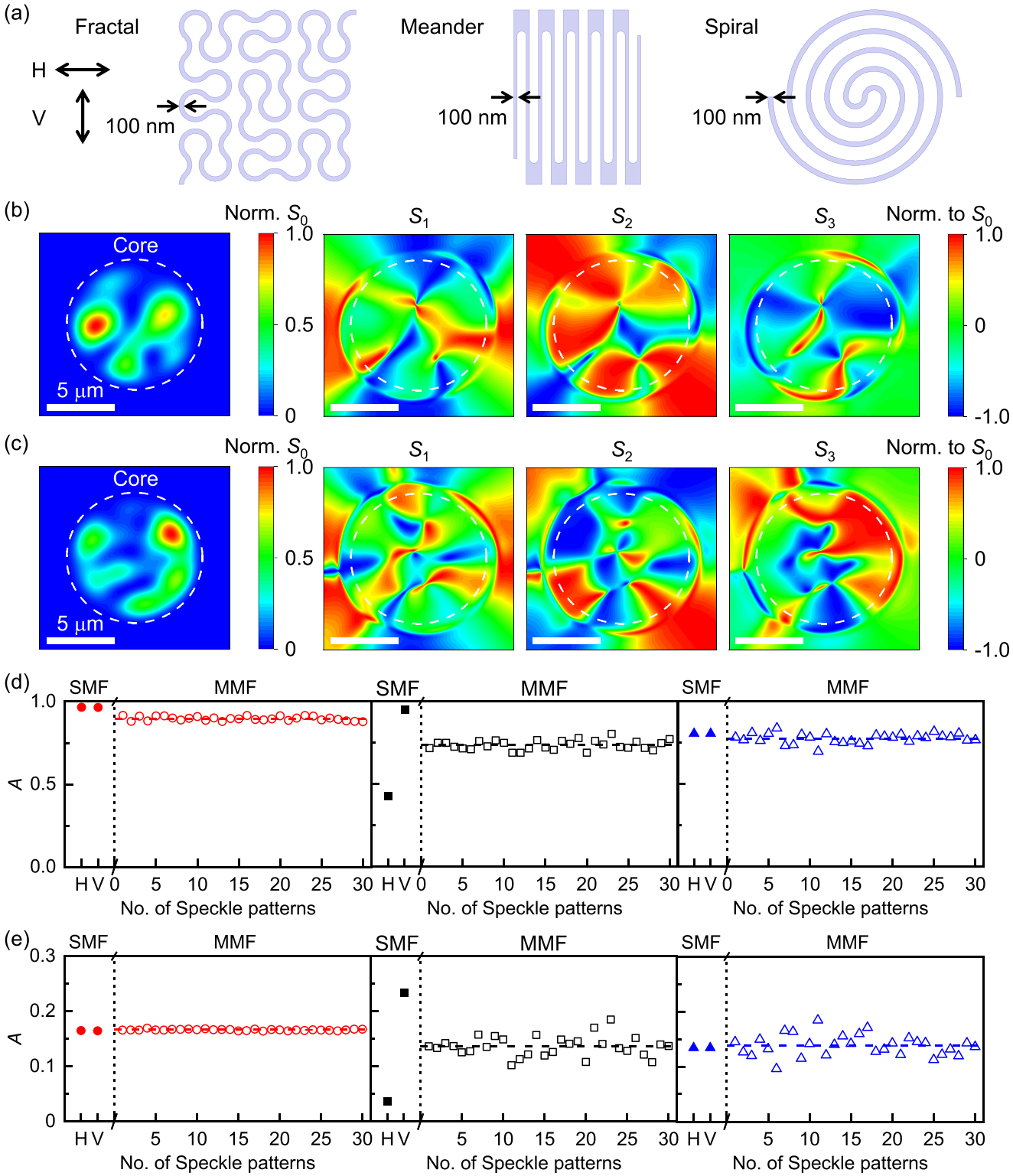

Figure 1. Speckles in multimode optical fiber (MMF) and the geometry-dependent optical absorption of superconducting nanowire single-photon detectors (SNSPDs). a) Three geometries of the SNSPDs: fractal, meander, and spiral, with the same width of the nanowire, 100 nm, and with the same fill factor, 0.26. b,c) Two example cases of simulated distributions of the Stokes parameters, S_0, S_1, S_2, and S_3, in the MMF, which supports 236 guiding modes in total. We superpose the first 20 vectorial modes with random amplitudes and random phases. The white dashed lines show the interfaces between the cores and the cladding layers. d) Simulated optical absorptance, A, of the of the fractal, meander, and spiral SNSPDs. An optical cavity is integrated to enhance A. The SNSPD patterned into the fractal geometry is insensitive to the speckles and can achieve high $\bar{A}$ with small perturbation, σ_A. e) Simulated optical absorptance, A, of the fractal, meander, and spiral free-standing SNSPDs, with different speckle patterns in the MMF. The SNSPD

patterned into the fractal geometry is insensitive to the speckles. In d) and e), A of the SNSPDs coupled with standard single-mode optical fibers (SMFs) are also simulated and presented, and each horizontal dashed line shows the average optical absorptance, $\bar{A}$. H and V, as shown in **a**, denote the two orthogonal states of polarization in the SMF.

by blackbody radiation coupled into the detector. See Section SIII (Supporting Information) for more detailed considerations about the design of the package. Figure 2d presents a photograph of the home-designed chip package.

We used two types of light sources to measure SDE* and/or SDE of the MMF-coupled fractal SNSPD and made a comparison. One was a quasi-coherent source, SuperK filtered by a monochromator; and another was a coherent light source, Santec continuous-wave tunable semiconductor laser with a linewidth of 500 kHz. The coherent light source generates more speckles than the quasi-coherent light source. See the infrared images in Figure S6 (Supporting Information). As the fractal SNSPD was configured into a 36 cascaded 2-SNAP, which generated afterpulses in addition to dark counts,[34] SDE is defined as the true system detection efficiency with both the dark counts and the afterpulses excluded and was experimentally measured by time-correlated photon counting. On the other hand, SDE* does not exclude the afterpulses but only excludes the dark counts and was experimentally measured by a counter of voltage pulses. We note that at high bias current, the values of SDE and SDE* are close. Another important point in our experimental methodology is that we want to excite as many guiding modes in the MMF as possible. To do so, we adjusted the position and tilted angle of the collimator to maximize the spot size at the output facet of the MMF, and measured the beam profile at the output facet using a beam profiler (**Figure 3a**). We note that this tilted excitation was similarly used in Ref. [37]. We ensured that the spot size (defined as the diameter in which the intensity is $1/e^2$ of the maximum intensity) is close to core diameter, 50 μ m. We note that directly connecting a piece of SMF with the MMF would not generate much of the high-order guiding modes in the MMF so that the spot size at the output facet would be smaller, and this method may lead to an overestimated SDE because the coupling between the smaller-size mode(s) and the photosensitive region becomes incorrectly simpler. We imaged the speckle patterns at the facet of the MMF excited in several ways using an infrared CCD camera, and Figure S6 (Supporting Information) presents these images.

Figure 3a presents the experimental setup for measuring SDE of the MMF-coupled fractal SNSPD using SuperK with a monochromator. Four calibrated neutral density filters (NDFs) were used to attenuate light. After attenuation, light was coupled into a step-index MMF with a core diameter of 50 μ m through a collimator. The resulting beam profile at the facet of the MMF was measured, without inserting the four NDFs, and is presented in Figure 3b. The resolution of the beam profiler in one direction is 0.6 μ m. The packaged device was mounted in a 0.1-W close-cycled Gifford-McMahon cryocooler with the base temperature of 2.5 K. Figure 3c presents measured SDE without and with the filter. The SDE without the filter peaked at 1530 nm. The measured SDE is $78 \pm 2\%$ at the bias current of 22.3 μ A. The SDE with filter peaked at 1540 nm. The measured SDE is $64 \pm 1\%$ at the bias current of 22.3 μ A. We present the detailed calculations of the uncertainties in Section SV (Supporting Information). Figure 3d presents measured dark-count rate (DCR) and false-count rate (FCR). The DCR is measured with the MMF feedthrough shielded by aluminum foil. At the bias current of 22.3 μ A, DCR and FCR without filter are 1.0×10^4 cps and 1.3×10^4 cps, respectively. The DCR and FCR with the filter are 1.9×10^2 cps and 2.1×10^2 cps, respectively. The filter significantly suppressed the DCR and FCR, and also added

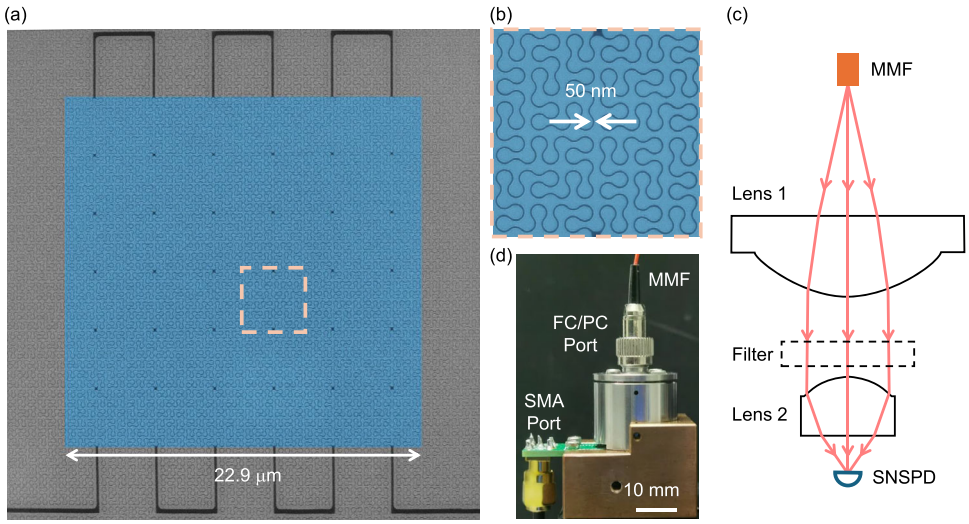

Figure 2. Large-area fractal superconducting nanowire single-photon detector (SNSPD) coupled with multimode optical fiber (MMF). a) A false-colored scanning-electron micrograph (SEM) of the fractal SNSPD, imaged after e-beam lithography and resist development but before reactive-ion etching. The photosensitive area is 22.9 μ m × 22.9 μ m. The detector is composed of 36 cascaded structures in the dashed box. b) A zoom-in view of the nanowire, corresponding to the dashed box in (a). The width of the nanowire is 50 nm. c) Schematics of the dual-lens optical system for beam compression. d) Photograph of the chip package pigtailed with a MMF cable.

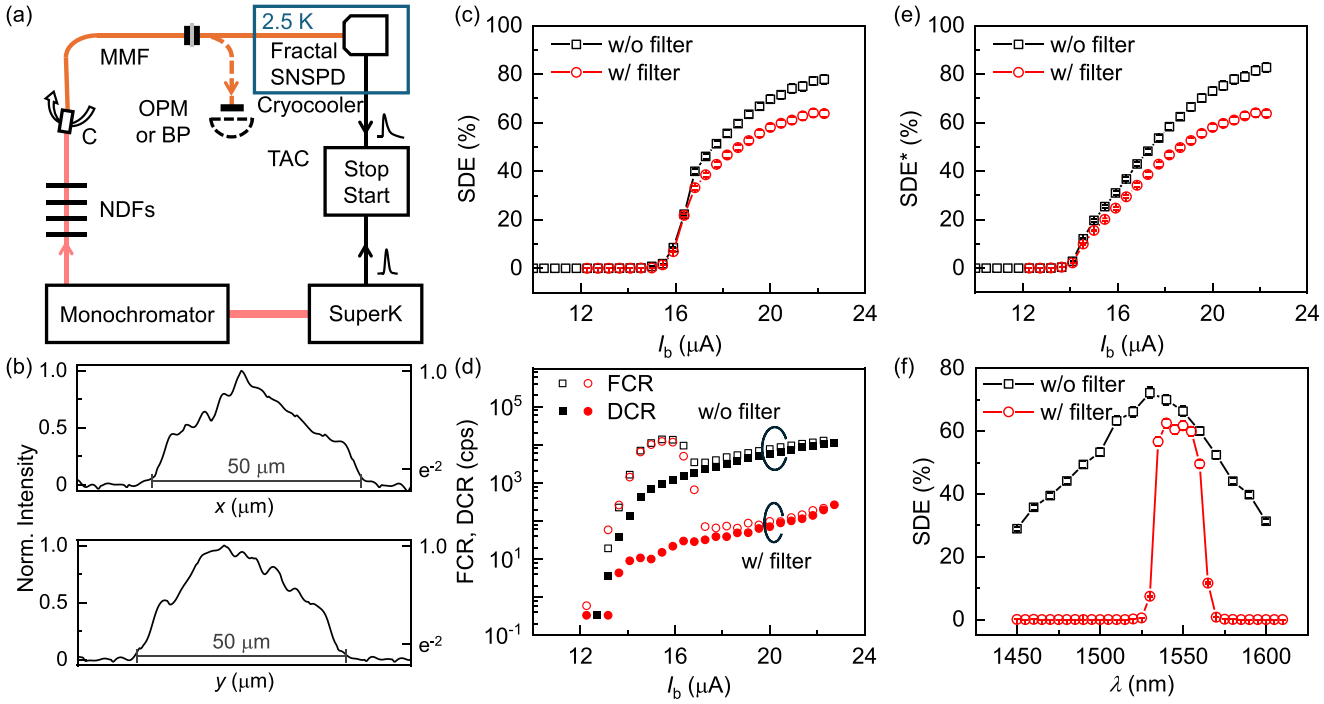

Figure 3. Measurements of the system detection efficiency using a quasi-coherent light source. a) Schematics of the experimental setup for measuring SDE. MMF, multimode optical fiber; OPM, optical power meter; BP, beam profiler; C, collimator; NDF, neutral density filter; TAC, time-to-amplitude converter. b) Normalized intensity along the *x* and *y* directions of the output beam of the MMF with a 50-μ m core diameter, measured by the beam profiler. c) Measured SDE at the wavelength of 1530 nm, as a function of the bias current, I_b. d) Measured dark-count rate (DCR) and false-count rate (FCR), as a function of the bias current, I_b, with and without the optical band-pass filter in the chip package. e) Measured SDE* at the wavelength of 1530 nm, as a function of the bias current, I_b. f) Measured spectrum of SDE, at a bias current of 20.9 μ A, with and without the optical band-pass filter in the chip package.

optical loss in its passing band, but, overall, noise-equivalent power (NEP, NEP $= \frac{h\nu}{SDE}\sqrt{2FCR}$, where $h\nu$ is photon energy) of the fractal SNSPD was decreased by adding the filter to the package. See Figure S7 (Supporting Information) for more detailed comparison of NEP with and without the filter. Figure 3e presents the measured SDE*.[34] At the bias current of 22.3 μ A, SDE* without and with the filter are 83 ± 2% and 64 ± 1%, respectively. In comparison, we directly connected a piece of single-mode fiber with the MMF, and SDE and SDE* were measured at the wavelength of 1540 nm to be 79 ± 2% and 79± 2%, respectively, with the optical filter mounted. Figure 3f presents the measured spectrum of SDE without and with filter at the bias current of 20.9 μ A. The full width at half maxima (FWHM) of the spectrum of SDE without the filter is 135 nm.

Figure 4a presents the experimental setup for measuring SDE* of the MMF-coupled fractal SNSPD using the CW laser. Three calibrated variable optical attenuators (VOAs) were used to attenuate light. After attenuation, light was coupled into the step-index MMF with a core diameter of 50 μ m through a collimator. The resulting beam profile at the facet of MMF was measured, without using the three VOAs, and is presented in Figure 4b. Figure 4c presents measured SDE* without and with filter. The SDE* without filter peaked at 1530 nm. The measured SDE is 76 ± 3% at the bias current of 22.3 μ A. The SDE* with filter peaked at 1540 nm. The measured SDE is 57 ± 3% at the bias current of 22.3 μ A. In comparison, we directly connected a piece of SMF with the MMF, and SDE* was measured at the wavelength of 1540 nm to be 81± 4% with the optical filter mounted. SDE* measured with the coherent source is quite consistent with that measured with the quasi-coherent source, also evidencing that the fractal SNSPDs are insensitive to speckles.

Figure 5 presents the properties in the time domain of the MMF-coupled SNSPD. Figure 5a is an oscilloscope trace of an output voltage pulse after being amplified by a low-noise cryogenic RF amplifier. The exponential fitting of the falling edge shows a e^{-1} time constant of 30 ns. We measured timing jitter of the device using a femto-second laser at the central wavelength of 1560 nm, a fast photodetector with 3-dB bandwidth of 40 GHz, and a real-time oscilloscope with a bandwidth of 4 GHz. Figure 5b presents timing jitter, as a function of I_b, and the lowest timing jitter is 42 ps at $I_b = 22.3$ μ A. The corresponding histogram of the time-delay as well as the Gaussian fitting is presented in Figure 5c. We note that the measured value of timing jitter, 42 ps, also includes the modal-dispersion-induced timing jitter of a 3-meter-long MMF, not only the electronic timing jitter of the SNSPD.

4. Conclusion

We compare our results with those reported in literature prior to our work, as listed in **Table** 1. For SDE, we have achieved the highest SDE, 76 ± 3% (SDE*) for the coherent light source and 78 ± 2% for the quasi-coherent light source, on a single-

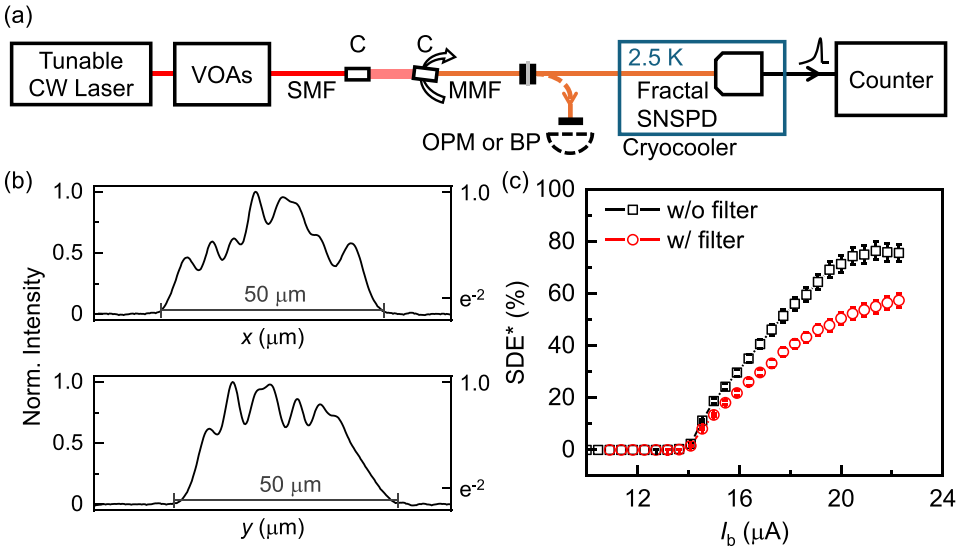

Figure 4. Measurements of the system detection efficiency using a coherent light source. a) Schematics of the experimental setup for measuring SDE*. CW, continuous wave; VOA, variable optical attenuator; MMF, multimode optical fiber; OPM, optical power meter; BP, beam profiler; C, collimator. b) Normalized intensity along the *x* and *y* directions of the output beam of the MMF with a 50-μ m core diameter, measured by the beam profiler. c) Measured SDE* at the wavelength of 1530 nm, as a function of the bias current, I_b.

element detector. In comparison, the next highest, 71%, was realized by Zhang et al.[21] in 2019 on a nine-pixel array, in which case the challenge on nanofabrication was less demanding. Our measured timing jitter, 42 ps, was much lower than what they reported, 150 ps. Compared with the work reported by Chang et al.[22] in 2019, timing jitter, 19.5 ps, was much lower than what we reported here; however, the device in that work was with a smaller area and SDE was lower. An additional note is that in our measurements, we inspected the modes in the MMF and maximized the profile of the mode field to ensure that more higher-order modes were excited. This inspection avoided the possible overestimation of SDE.

Although quite challenging, it is possible to further enhance the system detection efficiency of the MMF-coupled fractal SNSPDs. As the system detection efficiency is a product of η_c, A, and P_r, to achieve 100% system detection efficiency, we need to make all three efficiencies approach 100%. Specifically, 1) to achieve $\eta_c \approx 100\%$, the photosensitive area of the fractal SNSPD needs to be expanded to $> 30\ \mu$ m $\times$ 30 μ m according to our simulation, but at the cost of sacrificing the timing properties; 2) to achieve $A \approx 100\%$, the optical cavity based on the distributed Bragg reflectors should be fabricated accurately and with minimal deviations from the design in order to achieve high optical absorptance; 3) to achieve $P_r \approx 100\%$, the width of the nanowire should be reduced to ≈40 nm,[34] which may result in a more saturated internal quantum efficiency at high bias current, but this change of the width of the nanowire requires a careful re-design of the optical resonator to optimize A.

Our work also has important implications on modal noise. Since reported in 1978,[39] modal noise has intensively been investigated.[28,29,40] Goodman wrote in his book,[29] "this noise arises from the speckle intensity fluctuations when the propagating light passes through a transformation that restricts the portion of the light that is transmitted", and "certain types

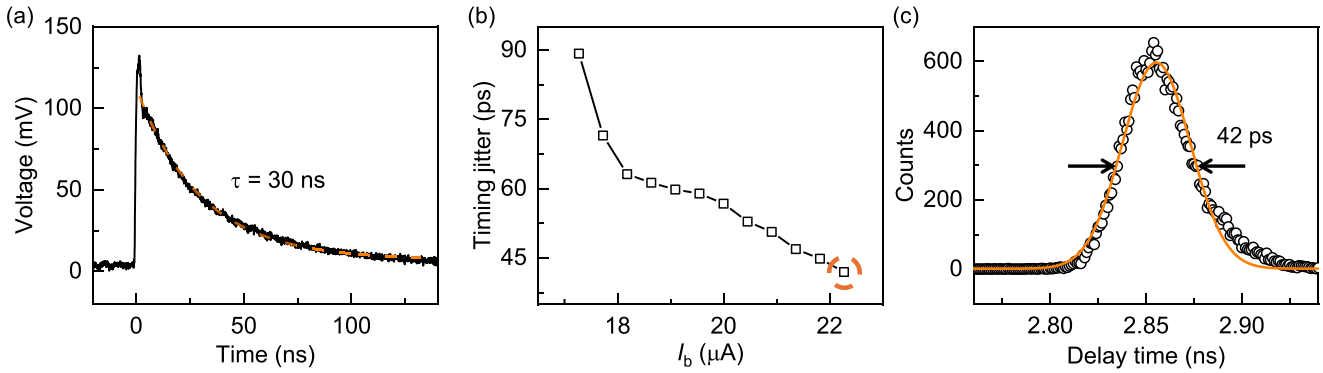

Figure 5. Properties in the time domain of the fractal superconducting nanowire single-photon detector (SNSPD) coupled with multimode optical fiber. a) Output voltage pulse of the SNSPD, after being amplified by a low-noise cryogenic RF amplifier. The exponential fitting of the falling edge shows a time constant of 30 ns. b) Measured timing jitter of the SNSPD, as functions of the bias current, I_b. c) Histogram of the time delay at the bias current of 22.3 μ A. The full width at half maxima of the Gaussian fitting is 42 ps.

Table 1. Comparison of the performances of the SNSPDs/SMSPDs[1] coupled with multimode optical fibers.

Reference	Structure	Area (μm^2)	Coupling method	MMF	Light source	SDE	DCR (cps)	Timing jitter (ps)
Zhang et al., 2014[19]	nanowire-meander	15×15	single-lens	50 μ m	coherent	56%	1×10^2	46
Zhang et al., 2015[20]	nanowire-meander	10×10	dual-lens	62.5 μ m	coherent	55%	1×10^1	–
Chang et al., 2019[22]	nanowire-meander	$\pi \times 10 \times 10$	–	50 μ m	coherent, with diffusers	50%	1×10^5	19.5
Zhang et al., 2019[21]	9-pixel nanowire-meander	$\pi \times 25 \times 25$	GRIN-lensed fiber	50 μ m (graded-index)	coherent	71%	3×10^4	150
Shcherbatenko et al., 2021[38]	microwire-meander	50×50	direct coupling	50 μ m	coherent	18%	1×10^2	–
Xu et al., 2021[23]	microwire-spiral	$\pi \times 25 \times 25$	GRIN-lensed fiber	50 μ m (graded-index)	coherent	63%	1×10^5	50
This work	nanowire-fractal	23×23	dual-lens	50 μ m (step-index)	coherent	$76 \pm 3\%$ (SDE*)	1×10^4	42
					quasi-coherent	$78 \pm 2\%$		

[1]SMSPDs: superconducting microwire single-photon detectors

of modal filtering devices" can cause modal noise. Specific to the SNSPDs discussed in this work, because their SDE may be polarization-dependent, and more generally, mode-dependent, SNSPDs can be viewed as modal filtering devices. The modal noise is geometry-dependent, and we uncover that fractal SNSPDs exhibit lower modal noise, compared with the meander and spiral geometries. Prior to our work, modal noise associated with SNSPDs has never been discussed; we think that modal noise should be very important in photon-counting optical communication systems[41,42] and deserves more research. In addition to SNSPDs, other nanostructured photodetectors may similarly have modal noises when they detect light coming from multiple spatial modes, and these detectors may include high-spectral photodetectors[43,44] and full-Stokes polarimetic photodetectors[45,46] that are integrated with meta-surfaces.

5. Experimental Section

Nanofabrication of the Fractal SNSPDs: Eight pairs of SiO_2/Ta_2O_5 alternating layers and a half of SiO_2 defect layer was deposited by ion beam-assisted deposition (IBD) on a 4-inch, 300-μ m-thick, double-side-polished silicon wafer. A 9-nm thick NbTiN film was sputtered at room temperature and diced the wafer into dies with a dimension of 20 mm × 19 mm. After making the metallic contact pads and markers by optical lithography, e-beam evaporation of titanium and gold, and lift-off, the nanowires were patterned by scanning-electron-beam lithography with a 50-nm-thick layer of hydrogen silsesquioxane (HSQ) and 100 kV accelerating voltage. The pattern from the HSQ layer was transferred, to the NbTiN layer after development using by CF_4 and O_2 reactive-ion etching. The top reflector was patterned by optical lithography, followed by depositing another half SiO_2 defect layer of the micro-cavity, and three pairs of Ta_2O_5/SiO_2 bi-layers using IBD. Then, lift-off was done. Finally, the chip was etched into the key-hole shape for self-aligned packaging. A 10-μ m-thick AZ 4620 was used as the photoresist. After patterning, inductively-coupled plasma etching was used to transfer the pattern to the stack, and removed the residual photoresist by immersing the chip in hot N-Methyl Pyrrolidone (NMP) at 95°C for 1 h.

Supporting Information

Supporting Information is available from the Wiley Online Library or from the author.

Acknowledgements

K.Z. and Y.M. contributed equally to this work. The authors thank Mr. Yi-fan Feng for technical assistance with the package design and thank Ms. Liping Du for lending us the infrared CCD camera. This work was supported by the Innovation Program for Quantum Science and Technology (No. 2023ZD0300100) and National Natural Science Foundation of China (NSFC) (62071322).

Conflict of Interest

The authors declare no conflict of interest.

Data Availability Statement

The data that support the findings of this study are available from the corresponding author upon reasonable request.

Keywords

detection efficiency, multimode optical fiber, polarization, speckle, superconducting nanowire single-photon detector, timing jitter

Received: March 13, 2024
Revised: May 14, 2024
Published online: May 23, 2024

[1] L. You, *Nanophotonics* **2020**, *9*, 2673.
[2] I. Esmaeil Zadeh, J. Chang, J. W. Los, S. Gyger, A. W. Elshaari, S. Steinhauer, S. N. Dorenbos, V. Zwiller, *Appl. Phys. Lett.* **2021**, *118*, 190502.
[3] H.-S. Zhong, H. Wang, Y.-H. Deng, M.-C. Chen, L.-C. Peng, Y.-H. Luo, J. Qin, D. Wu, X. Ding, Y. Hu, P. Hu, X.-Y. Yang, W.-J. Zhang, H. Li, Y. Li, X. Jiang, L. Gan, G. Yang, L. You, Z. Wang, L. Li, N.-L. Liu, C.-Y. Lu, J.-W. Pan, *Science* **2020**, *370*, 1460.
[4] L.-D. Kong, H. Wang, Q.-Y. Zhao, J.-W. Guo, Y.-H. Huang, H. Hao, S. Chen, X.-C. Tu, L.-B. Zhang, X.-Q. Jia, L. Kang, J. Chen, P.-H. Wu, *Nat. Photonics* **2023**, *17*, 65.

[5] X. Hu, N. Hu, K. Zou, Y. Meng, L. Xu, Y. Feng, *Laser Technol.* **2022**, *46*, 1.
[6] I. Esmaeil Zadeh, J. W. Los, R. Gourgues, V. Steinmetz, G. Bulgarini, S. M. Dobrovolskiy, V. Zwiller, S. N. Dorenbos, *APL Photonics* **2017**, *2*, 111301.
[7] J. Chang, J. Los, J. Tenorio-Pearl, N. Noordzij, R. Gourgues, A. Guardiani, J. Zichi, S. Pereira, H. Urbach, V. Zwiller, S. N. Dorenbos, I. Esmaeil Zadeh, *APL Photonics* **2021**, *6*, 036114.
[8] P. Hu, H. Li, L. You, H. Wang, Y. Xiao, J. Huang, X. Yang, W. Zhang, Z. Wang, X. Xie, *Opt. Express* **2020**, *28*, 36884.
[9] D. V. Reddy, R. R. Nerem, S. W. Nam, R. P. Mirin, V. B. Verma, *Optica* **2020**, *7*, 1649.
[10] K. Zou, Z. Hao, Y. Feng, Y. Meng, N. Hu, S. Steinhauer, S. Gyger, V. Zwiller, X. Hu, *Opt. Lett.* **2023**, *48*, 415.
[11] Y. Guan, H. Li, L. Xue, R. Yin, L. Zhang, H. Wang, G. Zhu, L. Kang, J. Chen, P. Wu, *Opt. Lasers Eng.* **2022**, *156*, 107102.
[12] J. Carpenter, C. Xiong, M. J. Collins, J. Li, T. F. Krauss, B. J. Eggleton, A. S. Clark, J. Schröder, *Opt. Express* **2013**, *21*, 28794.
[13] F. Xia, M. Gevers, A. Fognini, A. T. Mok, B. Li, N. Akbari, I. Esmaeil Zadeh, J. Qin-Dregely, C. Xu, *ACS Photonics* **2021**, *8*, 2800.
[14] F. Wang, F. Ren, Z. Ma, L. Qu, R. Gourgues, C. Xu, A. Baghdasaryan, J. Li, I. Esmaeil Zadeh, J. W. Los, A. Fognini, J. Qin-Dregely, H. Dai, *Nat. Nanotechnol.* **2022**, *17*, 653.
[15] H. Li, S. Chen, L. You, W. Meng, Z. Wu, Z. Zhang, K. Tang, L. Zhang, W. Zhang, X. Yang, X. Liu, Z. Wang, X. Xie, *Opt. Express* **2016**, *24*, 3535.
[16] B. E. Vyhnalek, S. A. Tedder, E. J. Katz, J. M. Nappier, in *Free-Space Laser Communications XXXI*, vol. *10910*, SPIE, Bellingham, WA **2019**, pp. 62–75.
[17] A. Schlehahn, S. Fischbach, R. Schmidt, A. Kaganskiy, A. Strittmatter, S. Rodt, T. Heindel, S. Reitzenstein, *Sci. Rep.* **2018**, *8*, 1340.
[18] L. V. Amitonova, T. B. Tentrup, I. M. Vellekoop, P. W. Pinkse, *Opt. Express* **2020**, *28*, 5965.
[19] L. Zhang, M. Gu, T. Jia, R. Xu, C. Wan, L. Kang, J. Chen, P. Wu, *IEEE Photon. J.* **2014**, *6*, 6802608.
[20] L. Zhang, C. Wan, M. Gu, R. Xu, S. Zhang, L. Kang, J. Chen, P. Wu, *Sci. Bull.* **2015**, *60*, 1434.
[21] C. Zhang, W. Zhang, L. You, J. Huang, H. Li, X. Sun, H. Wang, C. Lv, H. Zhou, X. Liu, Z. Wang, X. Xie, *IEEE Photon. J.* **2019**, *11*, 7103008.
[22] J. Chang, I. Esmaeil Zadeh, J. W. Los, J. Zichi, A. Fognini, M. Gevers, S. Dorenbos, S. F. Pereira, P. Urbach, V. Zwiller, *Appl. Opt.* **2019**, *58*, 9803.
[23] G.-Z. Xu, W.-J. Zhang, L.-X. You, J.-M. Xiong, X.-Q. Sun, H. Huang, X. Ou, Y.-M. Pan, C.-L. Lv, H. Li, Z. Wang, X.-M. Xie, *Photonics Res.* **2021**, *9*, 958.
[24] A. J. Kerman, E. A. Dauler, J. K. Yang, K. M. Rosfjord, V. Anant, K. K. Berggren, G. N. Gol'tsman, B. M. Voronov, *Appl. Phys. Lett.* **2007**, *90*, 101110.
[25] A. J. Kerman, E. A. Dauler, W. E. Keicher, J. K. Yang, K. K. Berggren, G. N. Gol'tsman, B. Voronov, *Appl. Phys. Lett.* **2006**, *88*, 111116.
[26] Y. Cheng, C. Gu, X. Hu, *Appl. Phys. Lett.* **2017**, *111*, 062604.
[27] N. Calandri, Q.-Y. Zhao, D. Zhu, A. Dane, K. K. Berggren, *Appl. Phys. Lett.* **2016**, *109*, 152601.
[28] J. W. Goodman, *JOSA* **1976**, *66*, 1145.
[29] J. W. Goodman, *Speckle phenomena in optics: theory and applications*, Roberts and Company Publishers, Greenwood Village, CO **2007**.
[30] H. Wu, C. Gu, Y. Cheng, X. Hu, *Appl. Phys. Lett.* **2017**, *111*, 062603.
[31] C. Gu, Y. Cheng, X. Zhu, X. Hu, in *Novel Optical Materials and Applications*, Optica Publishing Group, Washington, D.C. **2015**, Paper JM3A–10.
[32] X. Chi, K. Zou, C. Gu, J. Zichi, Y. Cheng, N. Hu, X. Lan, S. Chen, Z. Lin, V. Zwiller, X. Hu, *Opt. Lett.* **2018**, *43*, 5017.
[33] Y. Meng, K. Zou, N. Hu, X. Lan, L. Xu, J. Zichi, S. Steinhauer, V. Zwiller, X. Hu, *Opt. Lett.* **2020**, *45*, 471.
[34] Y. Meng, K. Zou, N. Hu, L. Xu, X. Lan, S. Steinhauer, S. Gyger, V. Zwiller, X. Hu, *ACS Photonics* **2022**, *9*, 1547.
[35] S. Dorenbos, E. Reiger, N. Akopian, U. Perinetti, V. Zwiller, T. Zijlstra, T. Klapwijk, *Appl. Phys. Lett.* **2008**, *93*, 161102.
[36] J. Huang, W. Zhang, L. You, X. Liu, Q. Guo, Y. Wang, L. Zhang, X. Yang, H. Li, Z. Wang, X. Xie, *Supercond. Sci. Technol.* **2017**, *30*, 074004.
[37] T. H. Wood, *Opt. Lett.* **1984**, *9*, 102.
[38] M. Shcherbatenko, M. Elezov, N. Manova, K. Sedykh, A. Korneev, Y. Korneeva, M. Dryazgov, N. Simonov, A. Feimov, G. N. Gol'tsman, D. Sych, *Appl. Phys. Lett.* **2021**, *118*, 181103.
[39] R. Epworth, in *Proc. 4th European Conf. on Optical Fiber Communication*, IEEE, Piscataway, NJ **1978**, pp. 492–501.
[40] G. C. Papen, G. M. Murphy, *J. Lightwave Technol.* **1999**, *17*, 817.
[41] H. Hao, Q.-Y. Zhao, Y.-H. Huang, J. Deng, F. Yang, S.-Y. Ru, Z. Liu, C. Wan, H. Liu, Z.-J. Li, H.-B. Wang, X.-C. Tu, L.-B. Zhang, X.-Q. Jia, X.-L. Wu, J. Chen, L. Kang, P.-H. Wu, *Light: Sci. Appl.* **2024**, *13*, 25.
[42] F. I. Khatri, B. S. Robinson, M. D. Semprucci, D. M. Boroson, *Acta Astronaut.* **2015**, *111*, 77.
[43] Y. Xiao, S. Wei, J. Xu, R. Ma, X. Liu, X. Zhang, T. H. Tao, H. Li, Z. Wang, L. You, Z. Wang, *ACS Photonics* **2022**, *9*, 3450.
[44] J. Yang, K. Cui, X. Cai, J. Xiong, H. Zhu, S. Rao, S. Xu, Y. Huang, F. Liu, X. Feng, W. Zhang, *Laser Photonics Rev.* **2022**, *16*, 2100663.
[45] A. Basiri, X. Chen, J. Bai, P. Amrollahi, J. Carpenter, Z. Holman, C. Wang, Y. Yao, *Light: Sci. Appl.* **2019**, *8*, 78.
[46] J. Bai, C. Wang, X. Chen, A. Basiri, C. Wang, Y. Yao, *Photonics Res.* **2019**, *7*, 1051.